The Planetary Science Journal, 5:133 (12pp), 2024 June https://doi.org/10.3847/PSJ/ad4350

Dimorphos's Orbit Period Change and Attitude Perturbation due to Its Reshaping after the DART Impact

Ryota Nakano[1,2], Masatoshi Hirabayashi[1,2], Sabina D. Raducan[3], Petr Pravec[4], Shantanu P. Naidu[5], Harrison F. Agrusa[6,7], Steven Chesley[5], Fabio Ferrari[8], Martin Jutzi[3], Colby C. Merrill[9], Alex J. Meyer[10], Patrick Michel[6,11], Derek C. Richardson[7], Paul Sánchez[12], Peter Scheirich[4], Stephen R. Schwartz[13,14], Yun Zhang[15], Adriano Campo Bagatin[16], Po-Yen Liu[16], and Andrew F. Cheng[17]

[1] Daniel Guggenheim School of Aerospace Engineering, Georgia Institute of Technology, Atlanta, GA 30332, USA
[2] Department of Aerospace Engineering, Auburn University, Auburn, AL 36849, USA
[3] Space Research and Planetary Sciences, Physics Institute, University of Bern, Bern 3012, Switzerland
[4] Astronomical Institute of the Academy of Sciences of the Czech Republic, Fričova 298, Ondřejov, CZ-25165, Czech Republic
[5] Jet Propulsion Laboratory, California Institute of Technology, Pasadena, CA 91109, USA
[6] Université Côte d'Azur, Observatoire de la Côte d'Azur CNRS, Laboratoire Lagrange, Nice, France
[7] Department of Astronomy, University of Maryland, College Park, MD 20742, USA
[8] Department of Aerospace Science and Technology, Politecnico di milano Milan, 20256, Italy
[9] Sibley School of Mechanical and Aerospace Engineering, Cornell University, Ithaca, NY 14853, USA
[10] Smead Department of Aerospace Engineering Sciences, University of Colorado Boulder, 3775 Discovery Drive, Boulder, CO 80303, USA
[11] The University of Tokyo Department of Systems Innovation, School of Engineering, Tokyo, Japan
[12] Colorado Center for Astrodynamics Research, University of Colorado Boulder, 3775 Discovery Drive, Boulder, CO, USA
[13] Planetary Science Institute, Tucson, AZ 85719, USA
[14] Instituto de Fisica Aplicada a las Ciencias y las Tecnologias (IUFACyT), Universidad de Alicante, Ctra. Sant Vicent del Raspeig s/n, 03690 Sant Vicent del Raspeig, Alicante, Spain
[15] Department of Climate and Space Sciences and Engineering, University of Michigan, Ann Arbor, MI 48109, USA
[16] IUFACyT—DFISTS. Universidad de Alicante, Ctra. Sant Vicent del Raspeig s/n, 03690 Sant Vicent del Raspeig, Alicante, Spain
[17] Johns Hopkins University, Applied Physics Laboratory, Laurel, MD 20723, USA
Received 2023 September 29; revised 2024 April 21; accepted 2024 April 23; published 2024 June 7

Abstract

On 2022 September 26 (UTC), NASA's Double Asteroid Redirection Test (DART) mission achieved a successful impact on Dimorphos, the secondary component of the near-Earth binary asteroid system (65803) Didymos. Subsequent ground-based observations suggest a significant reshaping of Dimorphos, with its equatorial axis ratio changing from 1.06 to ∼1.3. Here we report the effects of this reshaping event on Dimorphos's orbit and attitude. Given the reported reshaping magnitude, our mutual dynamics simulations show that approximately 125 s of the observed 33 minute orbit period change after the DART impact may have resulted from reshaping. This value, however, is sensitive to the precise values of Dimorphos's post-impact axis ratios and may vary by up to 2 times that amount, reaching approximately 250 s within the current uncertainty range. While the rotational state of the body is stable at the currently estimated axis ratios, even minor changes in these ratios or the introduction of shape asymmetry can render its attitude unstable. The perturbation to Dimorphos's orbital and rotational state delivered by the impact directly, combined with any reshaping, leads to a strong possibility for a tumbling rotation state. To accurately determine the momentum enhancement factor (β) through measurements by the European Space Agency's Hera spacecraft and to evaluate the effectiveness of the kinetic deflection technique for future planetary defense initiatives, the effects of reshaping should not be overlooked.

Unified Astronomy Thesaurus concepts: Near-Earth objects (1092); Asteroid satellites (2207); Asteroid dynamics (2210); Two-body problem (1723); Asteroid rotation (2211); Gravitational interaction (669); Accelerating universe (12); Planetary science (1255)

1. Introduction

NASA's Double Asteroid Redirection Test (DART) was the first full-scale planetary defense test mission to demonstrate asteroid deflection by kinetic impact (Daly et al. 2023). Launched on 2021 November 24 (UTC), the DART spacecraft successfully impacted Dimorphos, the secondary component of the near-Earth binary asteroid system (65803) Didymos, on 2022 September 26 (UTC). Ground-based observations revealed that the impact reduced the orbit period by 33.0 ± 1.0 (3σ) minutes (Thomas et al. 2023). This corresponds to Dimorphos's orbital velocity change in the along-track direction, $\Delta V_T = 2.7 \pm 0.1\,\mathrm{mm\,s^{-1}}$ (Cheng et al. 2023). If Dimorphos has a bulk density of $\sim$2,400 $\mathrm{kg\,m^{-3}}$, the momentum enhancement factor, β, is estimated as $3.61^{+0.19}_{-0.25}$ (1σ; Cheng et al. 2023) although this estimate of β depends strongly on the unknown mass of Dimorphos, which will be measured by the Hera mission led by European Space Agency (ESA) in early 2027 (Michel et al. 2022), allowing the determination of the actual value of β .

Prior to the DART impact, reshaping of either or both Didymos and Dimorphos were suggested as one of the possible outcomes of the impact (Hirabayashi et al. 2017, 2019, 2022; Nakano et al. 2022; Raducan & Jutzi 2022; Richardson et al. 2022). Given the fast spin period of 2.26 hr of Didymos, close to the structural spin limit for a cohesionless rubble-pile body

(e.g., Pravec et al. 2016; Zhang et al. 2017, 2021), Didymos's reshaping could be triggered by the impact-related perturbations, such as ejecta falling onto its surface (e.g., Hirabayashi et al. 2017). Dimorphos's reshaping could occur as a direct result of the impact. A pre-impact numerical model suggested that the impact could deform Dimorphos globally, beyond just forming a crater, depending on the structural strength of the body (e.g., Raducan & Jutzi 2022).

Such reshaping modifies the mutual potential between the bodies, which leads to a modification of Dimorphos's orbit period. Nakano et al. (2022) reported that even a slight shape change in either body, on the order of a few meters, could induce an orbit period change comparable to the required ground-based observation accuracy (i.e., 7.3 s; Rivkin et al. 2021; Chabot et al. 2024). If this reshaping effect is neglected, the effect of the kinetic deflection technique could be erroneously interpreted, potentially leading to an underestimation or overestimation of β (Nakano et al. 2022). Determining the magnitude of reshaping is, therefore, crucial to discern the orbit period change induced by reshaping and by the kinetic impact and to obtain an accurate β. However, constraining the magnitude of reshaping is a challenging task without in situ spacecraft measurements. Any reshaping of Didymos could readily be constrained by a corresponding change to its spin rate due to the conservation of angular momentum (Hirabayashi et al. 2017). For Dimorphos, the accuracy of post-impact ground-based observations dictates the accuracy of constraints for its reshaping. The degree of accuracy achievable through ground-based observations was uncertain before the impact.

As of this writing, the reshaping of Didymos has not been constrained as its spin period has shown no discernible change since the pre-impact period (J. Ďurech & P. Pravec et al. 2024, in preparation). In contrast, numerous efforts in observing the Didymos system indicate the possibility of post-impact reshaping of Dimorphos. While the post-impact shape cannot be determined directly from the ground, measuring the brightness variations of the system as Dimorphos rotates around Didymos (i.e., secondary rotational lightcurve) provides a way to infer Dimorphos's equatorial axis ratio, a_s/b_s. A secondary rotational lightcurve deduced from high-quality photometric observations suggests that a_s/b_s could be anywhere between 1.1 and 1.4 (Pravec et al., in review), a significant difference from its pre-impact value, 1.06 ± 0.03 (Daly et al. 2024). Furthermore, a planar dynamical model replicating over 5 months of post-impact mutual event observations also leads to a similar axis ratio, $a_s/b_s = 1.300 \pm 0.010$, as well as the polar axis ratio of $b_s/c_s = 1.3 \pm 0.2$ (Naidu et al. 2024). While acknowledging that these estimates of axis ratios rely on simplifying assumptions, such as Dimorphos being close to an ellipsoidal shape and tidally locked with low libration amplitude and having uniform mass distributions, they are generally consistent with recent impact simulation results suggesting a_s/b_s of up to $\sim$1.2 (Raducan et al. 2024).

Based on the observational and numerical results, this work aims to quantify the orbit period change and attitude perturbation of Dimorphos induced solely by its reshaping. Following Nakano et al. (2022), we generate synthetic shape models of Dimorphos in its reshaped form inferred from recent impact simulations (e.g., Raducan & Jutzi 2022; Raducan et al. 2022, 2024) and propagate the mutual dynamics of the nominal system before the DART impact. We explore a wide range of a_s/b_s, from 1.1 to 1.5, thoroughly encompassing the values estimated from the ground-based observations and impact simulation. This magnitude of reshaping was outside of the range considered in the earlier studies (Hirabayashi et al. 2019; Nakano et al. 2022). It is worth noting that this work will specifically determine the reshaping-induced orbit period change, one of the components contributing to the observed total period change. Whether the reshaping of Dimorphos occurs directly or through secondary processes, it is the kinetic impact from DART that initiates the chain of events. The outcomes of this study do not undermine the remarkable achievements of the DART mission but emphasize the necessity for a careful assessment to precisely estimate β and accurately evaluate the effectiveness of the kinetic deflection technique for future planetary defense initiatives. For more discussion on the pre- and post-impact dynamics of the Didymos system, beyond the effects of Dimorphos's reshaping, see Richardson et al. (2024).

Table 1
Dynamics-related Parameters of the Nominal Pre-impact Didymos System

Parameter	Pre-impact Value	Reference/Note
Pre-impact separation (m)	1219	Updated since Thomas et al. (2023)
System mass (kg)	5.6×10^{11}	Daly et al. (2023)
Didymos's dimension (m)		
- Major axis, $2\,a_p$	849	Daly et al. (2023)
- Intermediate axis, $2\,b_p$	851	Daly et al. (2023)
- Minor axis, $2\,c_p$	620	Daly et al. (2023)
Didymos's bulk density (kg/m^3)	2400	Daly et al. (2023)
Didymos's spin period (hr)	2.26	Pravec et al. (2006)
Dimorphos's dimension (m)		
- Major axis, $2\,a_s$	177	Daly et al. (2023)
- Intermediate axis, $2\,b_s$	174	Daly et al. (2023)
- Minor axis, $2\,c_s$	116	Daly et al. (2023)
Dimorphos's bulk density (kg/m^3)	2400	Daly et al. (2023)
Dimorphos's orbit period (hr)	11.921 481	Updated since Thomas et al. (2023)
Dimorphos's spin period (hr)	11.921 481	Assumed

2. Investigation Approach

Following Nakano et al. (2022), our investigation is twofold. First, we generate synthetic shape models of the reshaped Dimorphos. The synthetic shape models explore a wide range of axis ratios, $1.1 \leqslant a_s/b_s \leqslant 1.5$ and $0.7 \leqslant b_s/c_s \leqslant 2.1$, possible under a physically plausible, impact-induced reshaping mode of Dimorphos inferred from impact simulations. Second, we propagate the mutual dynamics using a finite-element-method (FEM) approach, mutual dynamics model for each synthetic shape model. To characterize specifically the effects of Dimorphos's reshaping, the simulations start from the nominal pre-impact state (Table 1). Importantly, we do not consider the momentum and torque imparted by the DART spacecraft and ejecta, which result in additional perturbations on the mutual dynamics, assuming that the reshaping and impact effects are independent (Nakano et al. 2022). The validity of this assumption is further discussed in Section 4.

2.1. Mutual Dynamics Model and Nominal Pre-impact Didymos System

The proximity and irregular shapes of Didymos and Dimorphos induce strong spin–orbit coupling, which requires

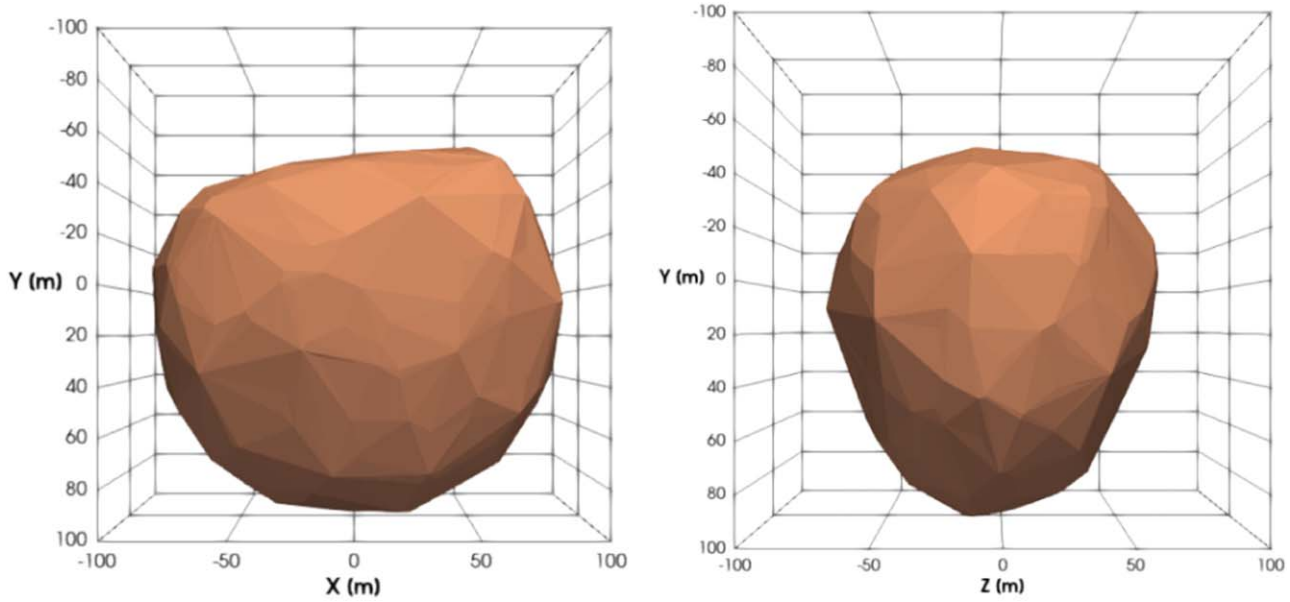

Figure 1. Post-impact shape model of Dimorphos based on smoothed particle hydrodynamics (SPH) impact simulation results: (left) top-down view and (right) side view. The DART spacecraft approached approximately along Dimorphos's intermediate axis (i.e., *Y*-axis in the figure) from negative to positive direction and impacted near the center of figure of the body.

the use of sophisticated numerical models to fully describe their mutual dynamics (e.g., Maciejewski 1995; Scheeres 2009). To describe this complex, coupled mutual dynamics, known as the Full Two-Body Problem (F2BP), we employ an FEM-approach F2BP (hereafter F2BPFEM; Nakano et al. 2022) model. In this FEM approach, FEM four-node mesh models of the primary and secondary are constructed from typical shape models consisting of triangular facets. The mesh models in this study are assumed to be rigid bodies with uniform mass distribution over their entire volumes. However, the meshes can account for mass distribution by changing the densities of tetrahedron elements. Using a bilinear interpolation technique, the mutual potential between a tetrahedral element in the primary and that in the secondary is first approximated and assembled at the end to obtain the total value of the mutual potential (Yu et al. 2019; Gao et al. 2021). Nakano et al. (2022) showed that the F2BPFEM model provides results consistent with a well-validated F2BP model, General Use Binary Asteroid Simulator (Davis & Scheeres 2021), which has been used in DART-related dynamics studies (e.g., Agrusa et al. 2020, 2021; Meyer et al. 2021; Richardson et al. 2022; Meyer et al. 2023a, 2023b; Cheng et al. 2023; Richardson et al. 2024).

In Table 1, we present the key dynamical parameters of the Didymos system prior to the DART impact. These parameters place the pre-impact system in a dynamically relaxed, equilibrium state, wherein Dimorphos's major axis points toward Didymos with a negligibly small libration amplitude (Agrusa et al. 2021). We refer to this configuration as the nominal system and do not consider uncertainties associated with each parameter. The FEM shape models are constructed from the dynamically equivalent equal-volume ellipsoids (DEEVEs) of Didymos and Dimorphos, with their dimensions listed in Table 1. This choice is made because of the limitations of current spacecraft-derived shape models, which only partially resolve surface features (Cheng et al. 2023; Daly et al. 2023). Using the DEEVEs yields sufficiently accurate results, given all uncertainties in the shapes and mass distributions, for example. We note that the pre-impact separation and Dimorphos's orbit period listed in Table 1 are the revised values since the initial post-impact reports (Thomas et al. 2023). The parameters in Table 1 are further refined and reported in Richardson et al. (2024) and Chabot et al. (2024). These parameter updates do not significantly alter the results of this investigation.

2.2. Synthetic Shape Models of a Reshaped Dimorphos

The ground-based observations and impact simulations suggest similar $a_s/b_s \sim 1.3$ (Pravec et al., in review; Naidu et al. 2024; Raducan et al. 2024), which means that the body is significantly elongated compared to the pre-impact oblate shape. To generate the synthetic shape models of a reshaped Dimorphos, simply changing the axis ratios of the oblate ellipsoid is one approach. However, this ignores physical processes that Dimorphos might have gone through after the DART impact and potentially misses important effects of reshaping including perturbations to its attitude state. We therefore employ a higher-fidelity approach, in which we consider a physically plausible reshaping mode of Dimorphos inferred from impact simulations in order to capture the potential effects accurately.

Figure 1 illustrates the post-impact Dimorphos shape model rendered based on smoothed particle hydrodynamics (SPH) impact simulation results, which closely reproduce the observed outcomes of the DART impact, including the orbit period change, total ejecta mass, and ejecta morphology (Raducan et al. 2024). We observe deformation across a relatively large area around the impact site (instead of a typical impact crater), owing to Dimorphos's low cohesive strength estimated to be a few Pascal (Barnouin et al. 2023; Raducan et al. 2024). The hemisphere opposite from the impact site exhibits no change in the SPH simulation results though a small change may occur as the shape adjusts to its minimal energy configuration for a given angular momentum (Liu et al. 2023).

This impact-induced reshaping mode of Dimorphos can be well characterized by asymmetrically changing axis lengths of a triaxial ellipsoid. The DART spacecraft's incoming direction was approximately aligned with Dimorphos's intermediate axis

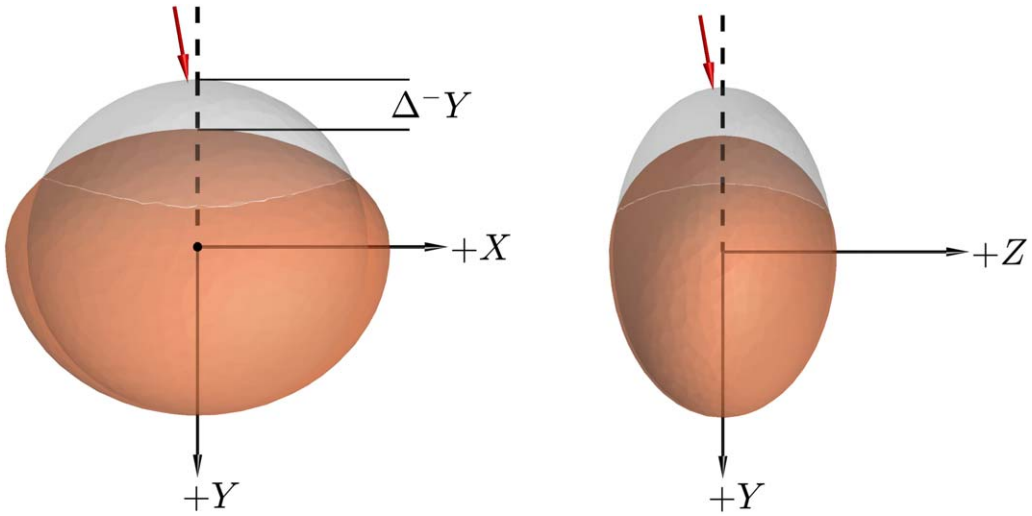

Figure 2. Synthetic shape model of reshaped Dimorphos (left) top-down view and (right) side view. The original shape model of Dimorphos is illustrated in gray. The red arrow indicates the DART impact condition. The change in the negative semi-intermediate axis length is denoted as $\Delta^{-}Y$. Although they are not shown, the changes in the semimajor and semiminor axes lengths (i.e., $\Delta^{\pm}X$ and $\Delta^{\pm}Z$) are also defined in a similar way.

although the impact location was slightly off from the center of the figure of Dimorphos (Daly et al. 2023). We thus consider that the impact instantaneously shortened the impact-side intermediate axis and lengthened major axes. We do not consider a change in the impact antipodal-side intermediate axis as such change is not observed in the SPH simulation results (Raducan et al. 2024). The minor axis could also undergo some changes in length, but whether it was shortened or lengthened is somewhat difficult to constrain. Thus, we consider that minor axes vary in both positive and negative directions such that the volume of Dimorphos before and after reshaping does not change. See Appendix A for more details. This constant volume assumption is supported by the fact that the estimated total ejecta mass accounts for only about 1% of Dimorphos's mass (e.g., Moreno et al. 2023; Roth et al. 2023; Ferrari et al. 2024).

As illustrated in Figure 2, we define a right-handed Cartesian body-fixed coordinate system $\{X, Y, Z\}$ such that the X-, Y-, and Z-axes align with the major, intermediate, and minor axes of the original body, respectively. The changes in the axis length in positive and negative directions are denoted as $\Delta^{\pm}X$, $\Delta^{\pm}Y$, and $\Delta^{\pm}Z$. This synthetic shape model-generation approach is consistent with Nakano et al. (2022). Importantly, the mutual dynamics are sensitive to small perturbations on the system's initial state, such as the initial velocities and rotation phases of the bodies (Agrusa et al. 2020). Therefore, particular care must be taken to ensure the consistency of the system's initial state throughout the simulations. To achieve this, for each synthetic shape model, we redefine the body-fixed coordinate system to align with the reshaped body's principal inertia axes centered at the mass center. Because the moment of inertia slightly varies for each shape, we also adjust its initial angular velocity to ensure that the angular momentum is conserved before and after reshaping (details in Appendix A). Impact simulations suggest that the majority of the reshaping is completed within a few hours following the DART impact, depending on how Dimorphos responds to the DART impact (e.g., Raducan & Jutzi 2022; Raducan et al. 2022, 2024). Due to this relatively short timescale compared to the orbit period, the results of this work remain largely unaffected, whether we consider time-variable or instantaneous reshaping.

3. Effects of Reshaping

3.1. Reshaping-induced Orbit Period Change, $\Delta P_{reshaping}$

Because we assume the reshaping and impact effects are independent, we can set the following relationship for the orbit period change:

$$\Delta P_{\rm observed} = \Delta P_{\rm kinetic} + \Delta P_{\rm reshaping}, \quad (1)$$

where $\Delta P_{\rm observed}$ is the orbit period change observed after the DART impact, which is ~33 min, and $\Delta P_{\rm kinetic}$ and $\Delta P_{\rm reshaping}$ are the orbit period change induced solely by the kinetic impact and solely by Dimorphos's reshaping, respectively. Any higher-order effects, such as binary hardening due to interactions with bound ejecta (Richardson et al. 2024), are ignored here.

We quantify $\Delta P_{\rm reshaping}$ by comparing the average stroboscopic orbit period of the reshaped Dimorphos to the nominal pre-impact orbit period (i.e., 11.921 481 hr). The stroboscopic orbit period is defined as the time required for a secondary to complete one full orbit about a primary relative to an inertial observer, resembling the method used in calculating the secondary's orbit period through lightcurve observations (Meyer et al. 2021). The stroboscopic orbit period closely correlates with the system's energy state—it remains constant when the system is in equilibrium but fluctuates when it is not in equilibrium and the secondary librates. In each simulation, we thus record the timings of reshaped Dimorphos crossing an arbitrary inertial plane perpendicular to the orbital plane and compute their average. We then subtract the nominal pre-impact orbit period from the average stroboscopic orbit period to obtain $\Delta P_{\rm reshaping}$.

3.1.1. Symmetric Reshaping

We first assume that the impact instantaneously shortened the intermediate axis and lengthened the major axis symmetrically in positive and negative directions (i.e., $\Delta^{+}X = \Delta^{-}X$). We also assume a symmetrical change in the minor axis (i.e., $\Delta^{+}Z = \Delta^{-}Z$) under the constant volume. In this symmetric impact-induced

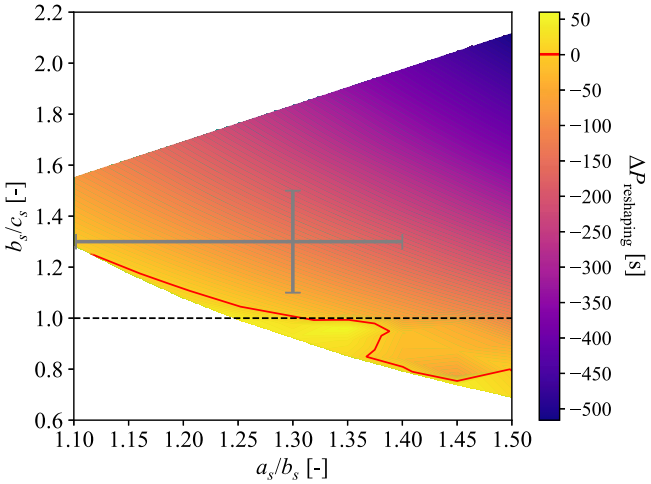

Figure 3. Reshaping-induced orbit period change, $\Delta P_{\mathrm{reshaping}}$, as a function of a_s/b_s and b_s/c_s. Reshaping is assumed to occur along the principal axes, and the post-impact shape is symmetrical about the Y-axis, as shown in Figure 2. The current estimates of the axis ratios a_s/b_s and b_s/c_s are indicated by the horizontal and vertical error bars, respectively (i.e., $1.1 \leqslant a_s/b_s \leqslant 1.4$ from Pravec et al., in review; $a_s/b_s = 1.300 \pm 0.010$ and $b_s/c_s = 1.3 \pm 0.2$ from Naidu et al. 2024). The dashed line indicates $b_s/c_s = 1.0$, below which the attitude becomes unstable. The red contour line indicates $\Delta P_{\mathrm{reshaping}} = 0$ s, which would extend toward the pre-impact axis ratios, $a_s/b_s \approx 1.06$ and $b_s/c_s \approx 1.47$ (Daly et al. 2024).

reshaping mode, the synthetic shape model's principal axes are shifted due to the center of mass displacement but not rotated with respect to the original principal axes. If this shift is left unaccounted for, the initial rotation state would not be consistent with the nominal condition (Table 1), introducing artifacts on the simulation results. As described in Section 2.2, this is addressed by appropriately redefining the body-fixed coordinate system. Later, we will explore off-principal-axis reshaping, where the new principal axes are both shifted and rotated from the original principal axes (Sections 3.1.3 and 3.2.2).

Figure 3 shows the reshaping-induced orbit period change, $\Delta P_{\mathrm{reshaping}}$, as a function of a_s/b_s and b_s/c_s that are permissible under the aforementioned impact-induced reshaping mode. We find that $\Delta P_{\mathrm{reshaping}}$ can range from -500 to 50 s over the range of a_s/b_s and b_s/c_s considered. Most shapes with $b_s/c_s \geqslant 1.0$ result in $\Delta P_{\mathrm{reshaping}} < 0$ s. In general, the larger the a_s/b_s and b_s/c_s are, the higher the significance of the reshaping effect (i.e., $\Delta P_{\mathrm{reshaping}}$ becomes more negative). Only a limited set of shapes having b_s/c_s close to 1 result in $\Delta P_{\mathrm{reshaping}} > 0$ s. On the other hand, shapes with $b_s/c_s < 1$ are attitude unstable as expected from rigid-body dynamics (see Section 3.2), and therefore, their stroboscopic orbit periods do not remain constant and fluctuate with various frequencies (Meyer et al. 2021). This leads to a variation in $\Delta P_{\mathrm{reshaping}}$ and thus unsmooth contours. While the axis ratios explored here are significantly larger than those of Nakano et al. (2022), the general effect of Dimorphos's reshaping is consistent.

In Figure 3, the horizontal error bars indicate the current estimates for a_s/b_s and b_s/c_s, respectively ($1.1 \leqslant a_s/b_s \leqslant 1.4$ from Pravec et al., in review; $a_s/b_s = 1.300 \pm 0.010$ and $b_s/c_s = 1.3 \pm 0.2$ from Naidu et al. (2024). If the post-impact Dimorphos's shape is exactly at the intersection of the vertical and horizontal error bars (i.e., $a_s/b_s = 1.3$ and $b_s/c_s = 1.3$), $\Delta P_{\mathrm{reshaping}}$ is approximately -125 s. If it falls within the uncertainty range, $\Delta P_{\mathrm{reshaping}}$ can vary from -250 to 10 s.

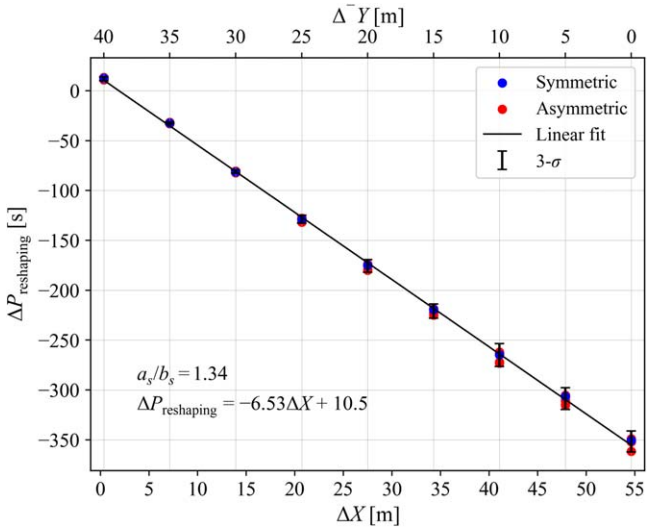

Figure 4. $\Delta P_{\mathrm{reshaping}}$ as a function of (bottom) ΔX and (top) ΔY. The equatorial axis ratio a_s/b_s is fixed at 1.34. The blue and red dots indicate $\Delta P_{\mathrm{reshaping}}$ due to symmetric and asymmetric reshaping, respectively. The black solid line indicates the linear fit for $\Delta P_{\mathrm{reshaping}}$ due to asymmetric reshaping.

3.1.2. Asymmetric Reshaping

We now relax the assumption of the symmetric reshaping and consider shapes that have asymmetry along the major and minor axes (i.e., $\Delta^+ X \neq \Delta^- X$ and $\Delta^+ Z \neq \Delta^- Z$). Because of, for example, the local surface curvature and distribution of boulders (Hirabayashi et al. 2024; Pajola et al. 2024; Raducan et al. 2024), the material ejection and reaccumulation at the surface are heterogeneous, leading to an asymmetric shape. Therefore, this resembles a more realistic reshaping condition.

Here, we specifically focus on $a_s/b_s = 1.34$ shapes and vary $\Delta^- Y$ from 0 to 40 m with a step of 5 m. For each $\Delta^- Y$, we generate ten synthetic shape models having different $\Delta^{\pm} X$ and $\Delta^{\pm} Z$. $\Delta^+ X$ and $\Delta^+ Z$ are uniform randomly selected under the constraints of $a_s/b_s = 1.34$ and constant volume. $\Delta^- X$ and $\Delta^- Z$ are defined, given $\Delta^+ X$ and $\Delta^+ Z$. In Figure 4, we plot $\Delta P_{\mathrm{reshaping}}$ as a function of $\Delta X = \Delta^+ X + \Delta^- X$ (bottom x-axis) and $\Delta^- Y$ (top x-axis). The blue and red dots indicate $\Delta P_{\mathrm{reshaping}}$ due to symmetric and asymmetric reshaping, respectively. The red dots gradually disperse as ΔX increases. However, the mean value for given ΔX and $\Delta^- Y$ is always consistent with $\Delta P_{\mathrm{reshaping}}$ from symmetric reshaping. This can also be seen from the linear fit indicated by the black solid line. These results suggest that the shape asymmetries along the major and minor axes only induce a minor difference in $\Delta P_{\mathrm{reshaping}}$, compared to the symmetric reshaping condition. Therefore, assuming the shape symmetry in the post-impact Dimorphos can predict $\Delta P_{\mathrm{reshaping}}$ with sufficient accuracy. This finding holds for the other a_s/b_s values too.

3.1.3. Off-principal-axis Reshaping

So far, we have described reshaping by modifying the principal axes of the pre-impact Dimorphos (i.e., X-, Y-, and Z-axes in Figure 2). However, the small in-plane and out-of-plane velocity components of the DART spacecraft (Daly et al. 2023), in addition to potential structural heterogeneity of Dimorphos, may lead to reshaping that does not perfectly align with the principal axes. In fact, the SPH impact simulation results show

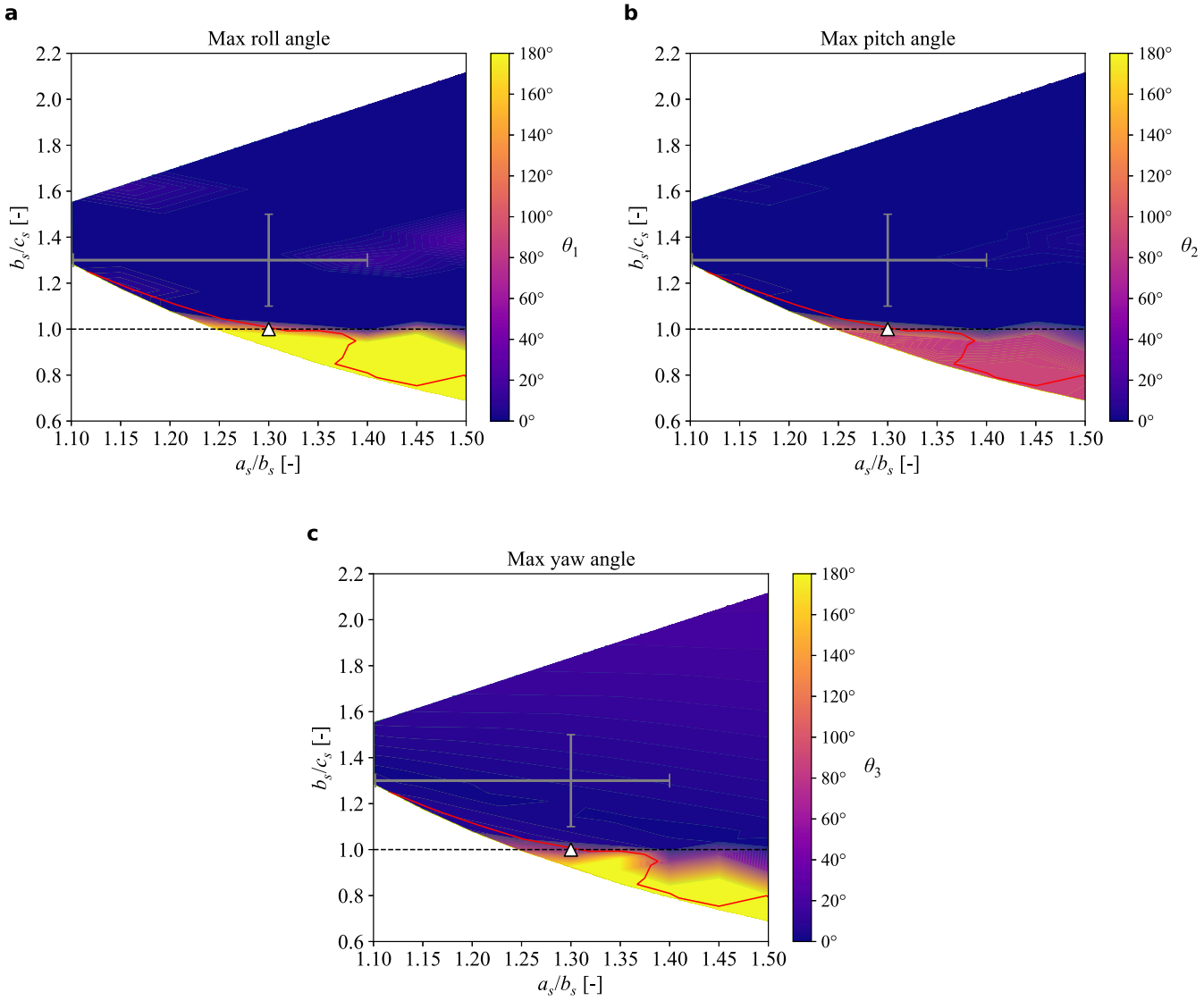

Figure 5. Maximum roll, pitch, and yaw amplitudes as a function of a_s/b_s and b_s/c_s. Reshaping is assumed to occur along the principal axes, and the post-impact shape has a symmetry about the Y-axis, as shown in Figure 2. The horizontal and vertical error bars indicate the current estimates of the axis ratios. The red contour line indicates $\Delta P_{\text{reshaping}} = 0$ s. The white triangle indicates the attitude-unstable shape whose time evolution of roll, pitch, and yaw angles are plotted in Figure 6.

such a feature, approximately 10° measured from the intermediate axis on the equatorial plane in Figure 1, for example (Raducan et al. 2024).

We thus conducted an additional investigation using synthetic shape models that capture off-principal-axis reshaping.[18] However, we found that the orbit period change due to off-principal-axis reshaping is consistent with that due to the axial reshaping (i.e., Section 3.1.1). This is because the global-scale reshaping (i.e., changing a_s/b_s from 1.06 to ∼1.3) is the dominant factor modifying the mass distributions within the system and, consequently, the mutual potential that ultimately governs the orbit period. Therefore, regardless of the axial or off-axial reshaping, the post-impact axis ratios a_s/b_s and b_s/c_s primarily determine the orbit period change. Notably, however, the off-principal-axis reshaping does cause a nonnegligible effect on the attitude state of Dimorphos. This is detailed in Section 3.2.2.

[18] See Section 3.2.2 for the details of the synthetic shape models.

3.2. Dimorphos's Attitude Perturbation

3.2.1. Symmetric Reshaping

The attitude state of Dimorphos can be quantified by using the 1-2-3 Euler angles: roll, pitch, and yaw (Agrusa et al. 2021). The roll, pitch, and yaw angles typically measure Dimorphos's rotation about its major, intermediate, and minor axes, respectively. However, because the axes may switch depending on magnitude of reshaping (e.g., when $b_s/c_s < 1.0$), we measure the angles with respect to $\{X, Y, Z\}$ axes that aligned with the major, intermediate, and minor principal axes of the pre-impact shape in this work. Because our simulations start from a dynamically relaxed state in which Dimorphos is tidally locked, these angles are initially at zero. Without any external perturbations on Dimorphos's attitude, the time evolution of these angles remains zero or always bounded within a few degrees and never becomes unstable (e.g., Agrusa et al. 2021; Richardson et al. 2022).

Figure 5 shows the maximum amplitudes in roll, pitch, and yaw angles attained by symmetrically reshaped Dimorphos

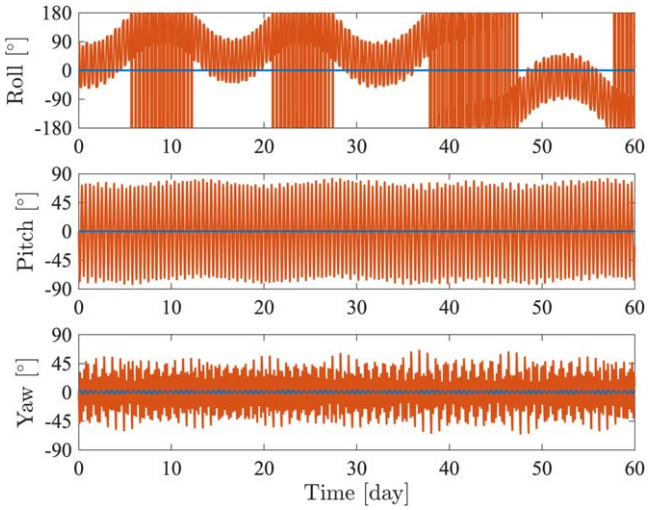

Figure 6. Time evolution of roll, pitch, and yaw angles. The blue and red lines denote the stable and unstable shapes, respectively. The stable shape has $a_s/b_s = 1.3$ and $b_s/c_s = 1.3$, and the unstable shape has $a_s/b_s = 1.3$ and $b_s/c_s = 1.0$.

(i.e., same shapes as in Section 3.1.1). In all three angles, most shapes show smaller than ∼20° amplitude. However, the shapes with $b_s/c_s \lesssim 1.0$ consistently exhibit attitude instability. As all three angles have high amplitudes, those shapes are likely chaotically tumbling, i.e., they are in a non-principal-axis rotation state. Figure 5 also plots the $\Delta P_{\rm reshaping} = 0$ s contour line found in Section 3.1.1. We observe that the shapes that lead to $\Delta P_{\rm reshaping} < 0$ s (and have $b_s/c_s > 1.0$) are generally stable, while the shapes that lead to $\Delta P_{\rm reshaping} \geqslant 0$ s are unstable (i.e., exceeding 90° amplitude) in at least one angle, if not tumbling.

Figure 6 plots the time evolution of the roll, pitch, and yaw angles for two shapes: both have the same a_s/b_s of 1.3 but different b_s/c_s, 1.3 and 1.0, which result in the stable and unstable attitude state, respectively. In the figure, the stable shape is colored in blue, and the unstable shape is colored in red. As expected from Figure 5, the stable shape shows no roll and pitch angles throughout the simulation. Although there is about 5° amplitude oscillation in yaw, it remains periodic and never becomes unstable. On the other hand, the unstable shape exhibits nonzero roll, pitch, and yaw angles. The roll angle is particularly perturbed and randomly oscillates back and forth between positive and negative angles with various amplitudes. The pitch and yaw oscillation start immediately after the reshaping event. The amplitude of pitch angle is relatively large yet bounded around 70°, while that of the yaw angle is bounded around 45°. Notably, although this shape is unstable in all three angles, the major axis still points toward Didymos on average, mimicking the tidally locked state, known as the barrel instability (Ćuk et al. 2020).

These results align with what we expect from rigid-body dynamics. The majority of post-impact shapes exhibit stability in their attitude states because the perturbation caused by reshaping, i.e., a sudden change in the moment of inertia tensor, is within a permissible range for the initial rotation state. However, in extreme reshaping conditions where there is a sudden swap of the intermediate and minor axes ($b_s/c_s < 1.0$), that is no longer the case, and such bodies become inherently unstable. Importantly, Dimorphos's attitude perturbation discussed here is induced solely by reshaping. Agrusa et al. (2021) reported that Dimorphos may become unstable after the DART impact, depending on the pre-impact Dimorphos shape and β, even without reshaping. Given the pre-impact shape ($a_s/b_s = 1.06 \pm 0.03$ and $b_s/c_s = 1.47 \pm 0.04$) and $\beta = 3.61^{+0.19}_{-0.25}$, as well as some amount of torque applied by the impact, such attitude instability, including the tumbling state, is highly plausible (Richardson et al. 2024). Our results here imply that Dimorphos reshaping would further increase the likelihood of attitude instability when both impact and reshaping are considered.

3.2.2. Off-principal-axis Reshaping

In Section 3.1.3, we investigated the effect of the off-principal-axis reshaping on the orbit period, which we determined to be consistent with the principal-axis reshaping. However, such off-principal-axis reshaping can cause a significant difference in Dimorphos's attitude state compared to the principal-axis reshaping.

We prepare a new set of synthetic shape models to investigate the effect of the off-principal-axis reshaping. Figure 7 shows an example shape model that represents Dimorphos undergoing off-principal-axis reshaping. While the shape model construction process is consistent with Section 2.2, two additional parameters, $\theta_{\rm in}$ and $\theta_{\rm out}$, are introduced, which describe the in-plane and the out-of-plane reshaping angles, respectively. Applying a sequence of rotation $\theta_{\rm in}$ and $\theta_{\rm out}$ to the original Cartesian coordinate system $\{X, Y, Z\}$, a new set of Cartesian coordinate system $\{X', Y', Z'\}$ can be established. The off-principal-axis reshaping is described along this new Cartesian coordinate system. Y'-axis is assumed to be shortened directly due to the impact, while X'-axis lengthens and Z'-axis varies to conserve the volume. We assume $\Delta^+X' = \Delta^-X'$ and $\Delta^+Z' = \Delta^-Z'$. We denote the equatorial and polar axis ratios based on the new principal axes as a_s'/b_s' and b_s'/c_s', respectively. The orientation of the new principal axes differs from that of the pre-impact shape model by $\theta_{\rm in}$ and $\theta_{\rm out}$. As outlined in Appendix A, this difference is taken into account during the simulation setup process in order to have a dynamically consistent initial state throughout the simulations.

Here we consider $a_s'/b_s' = 1.3$ with $\Delta^-Y' = 25$ m and systematically vary both $\theta_{\rm in}$ and $\theta_{\rm out}$ from 0° to 20°, with a step of 5°. This range for $\theta_{\rm in}$ and $\theta_{\rm out}$ thoroughly covers the angles observed in the impact simulation results (Raducan et al. 2024). For the shape with $\theta_{\rm in} = \theta_{\rm out} = 0°$, b_s'/c_s' is ∼1.2. Because the pre-impact shape is circular on the equatorial plane, a_s'/b_s' is always 1.3 regardless of $\theta_{\rm in}$. However, b_s'/c_s' slightly varies for different $\theta_{\rm out}$. Note that from Figure 5, we would expect that the body with $a_s'/b_s' = 1.3$ and $b_s'/c_s' = 1.2$ is stable in all three angles.

Figure 8 shows the maximum amplitudes in roll, pitch, and yaw angles as a function of $\theta_{\rm in}$ and $\theta_{\rm out}$. We find that while all three angles are zero when $\theta_{\rm in} = \theta_{\rm out} = 0°$ as expected, both nonzero $\theta_{\rm in}$ and $\theta_{\rm out}$ cause a considerable difference. Given the DART impact condition and the resulting reshaping mode of Dimorphos, in which one hemisphere reshapes more than the other hemisphere, the body would naturally tend to rotate about the major axis. With either $\theta_{\rm in}$ or $\theta_{\rm out}$ being nonzero, the roll angle is thus easily excited, resulting in the largest variation in the amplitude due to $\theta_{\rm in}$ and $\theta_{\rm out}$, compared to the other two angles. The amplitude in roll angle can reach as high as 45°. The pitch shows similar behavior to the roll, but its amplitude

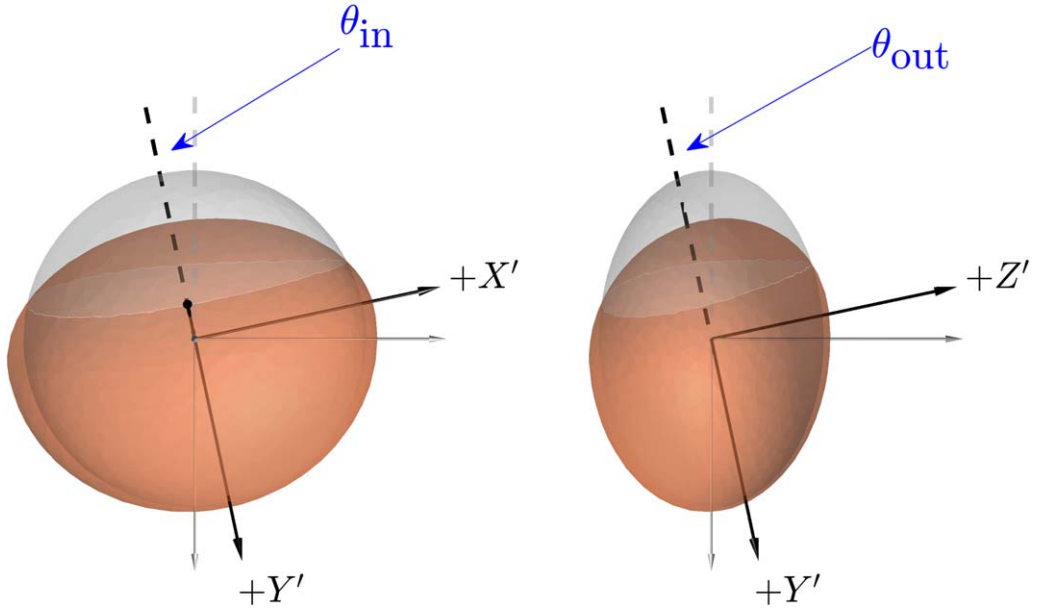

Figure 7. Synthetic shape model of Dimorphos undergoing off-principal-axis reshaping: (left) top-down view and (right) side view. $\theta_{\rm in}$ and $\theta_{\rm out}$ denote the in-plane and the out-of-plane reshaping angles, respectively. Applying a sequence of rotation $\theta_{\rm in}$ and $\theta_{\rm out}$ to the original Cartesian coordinate system $\{X, Y, Z\}$, a new set of Cartesian coordinate system $\{X', Y', Z'\}$ can be established, along which the reshaping is described.

reaches 20° at maximum at $\theta_{\rm in} = \theta_{\rm out} = 20°$. Both roll and pitch are sensitive to both $\theta_{\rm in}$ and $\theta_{\rm out}$. The yaw angle, on the other hand, shows a strong dependence only on $\theta_{\rm in}$ and not so much on $\theta_{\rm out}$, and its maximum amplitude is about 25°. It is important to note that after this off-principal-axis reshaping, the new principal axes do not align with the original principal axes. Dimorphos now spins about these new principal axes unless Dimorphos is in a chaotic tumbling state. Therefore, there will be a difference in the spin pole direction of Dimorphos constrained before the DART impact and that measured by the Hera spacecraft in the future.

4. Discussion and Conclusion

While ground-based observations and impact simulations suggest a post-impact equatorial axis ratio of Dimorphos a_s/b_s of $\sim$1.3, there remains a relatively large uncertainty mainly due to the unconstrained rotation state of the body. The exact axis ratios a_s/b_s and b_s/c_s are pending direct measurements by the Hera spacecraft that arrives at the system in late December 2026 (Michel et al. 2022). In this study, we thus considered a wide range of axis ratios, $1.1 \leqslant a_s/b_s \leqslant 1.5$ and $0.7 \leqslant b_s/c_s \leqslant 2.1$, and investigated the effects of reshaping on its orbit period and attitude state.

Our findings indicate that reshaping can induce a significant orbit period change ($\Delta P_{\rm reshaping}$), ranging from −500 to 50 s for the range of axis ratios considered in this work. Under the physically plausible, impact-induced reshaping mode inferred from recent impact simulations (e.g., Raducan et al. 2024), the majority of the shapes resulted in decreasing the orbit period, while a limited set of shapes led to increasing it. What ultimately drives this orbit period change is a subtle modification in the gravitational field between the two bodies due to reshaping. As such, we have also quantified the changes in Dimorphos's oblateness and ellipticity due to reshaping, similar to Nakano et al. (2022). Figure 9 presents $\Delta P_{\rm reshaping}$ for the case of symmetric reshaping as a function of the changes in the zonal and tesseral terms of degree 2, ΔC_{20} and ΔC_{22}, respectively, which encapsulate the dominant gravitational perturbations (details in Appendix B). The dashed line represents $\Delta C_{22} = 0.265\ \Delta C_{20}$, a theoretical boundary between positive and negative orbit period changes (Equation (B5)), while the red contour line denotes the $\Delta P_{\rm reshaping} = 0$ s from simulations. Despite the deviations between the two lines due to orbit period fluctuations arising from attitude instabilities of $b_s/c_s < 1.0$ shapes, the overarching trend aligns with the conclusion drawn from Figure 3—reshaping predominantly reduces orbit period, with only shapes characterized by $\Delta C_{22} \lesssim 0.265\ \Delta C_{20}$ exhibiting an increase. These results are consistent with previous studies and highlight the importance of accounting for reshaping when analyzing the post-impact orbit period of Dimorphos.

Considering the estimated axis ratios of $a_s/b_s = 1.300 \pm 0.010$ and $b_s/c_s = 1.3 \pm 0.2$ from the planar orbit-fitting analysis based on the mutual event observations (Naidu et al. 2024), $\Delta P_{\rm reshaping}$ can take a value from −200 to −50 s. If we consider the range of a_s/b_s estimated from the secondary lightcurve ($1.1 \leqslant a_s/b_s \leqslant 1.4$; Pravec et al., in review), $\Delta P_{\rm reshaping}$ can be −250 s. This implies that within the observed orbit period change of $\sim$33 min, as much as $\sim$4 min could be attributed to Dimorphos's reshaping, as opposed to being solely attributed to the momentum change caused by the DART impact and ejecta recoil.

$\Delta P_{\rm reshaping}$ of 4 min corresponds to about -0.347 mm s^{-1} of ΔV_T based on a simple Keplerian relationship. If our assumption that the effects of reshaping and impact are independent holds true, neglecting the reshaping effect would lead to an overestimation of ΔV_T. In fact, Richardson et al. (2024) recently reported a ΔV_T of -2.42 mm s^{-1} by considering the updated pre- and post-impact system parameters including Dimorphos's reshaping (see Table 2 in Richardson et al. 2024). Furthermore, Naidu et al. (2024) also estimate a slightly higher value, $\Delta V_T = -2.62$ mm s^{-1}, by accounting for the reshaping effect. These two new estimates are, respectively, 0.28 and 0.08 mm s^{-1} smaller than the value initially reported without accounting for the reshaping effect, -2.70 ± 0.10 (1σ) mm s^{-1} (Cheng et al. 2023). Considering the current

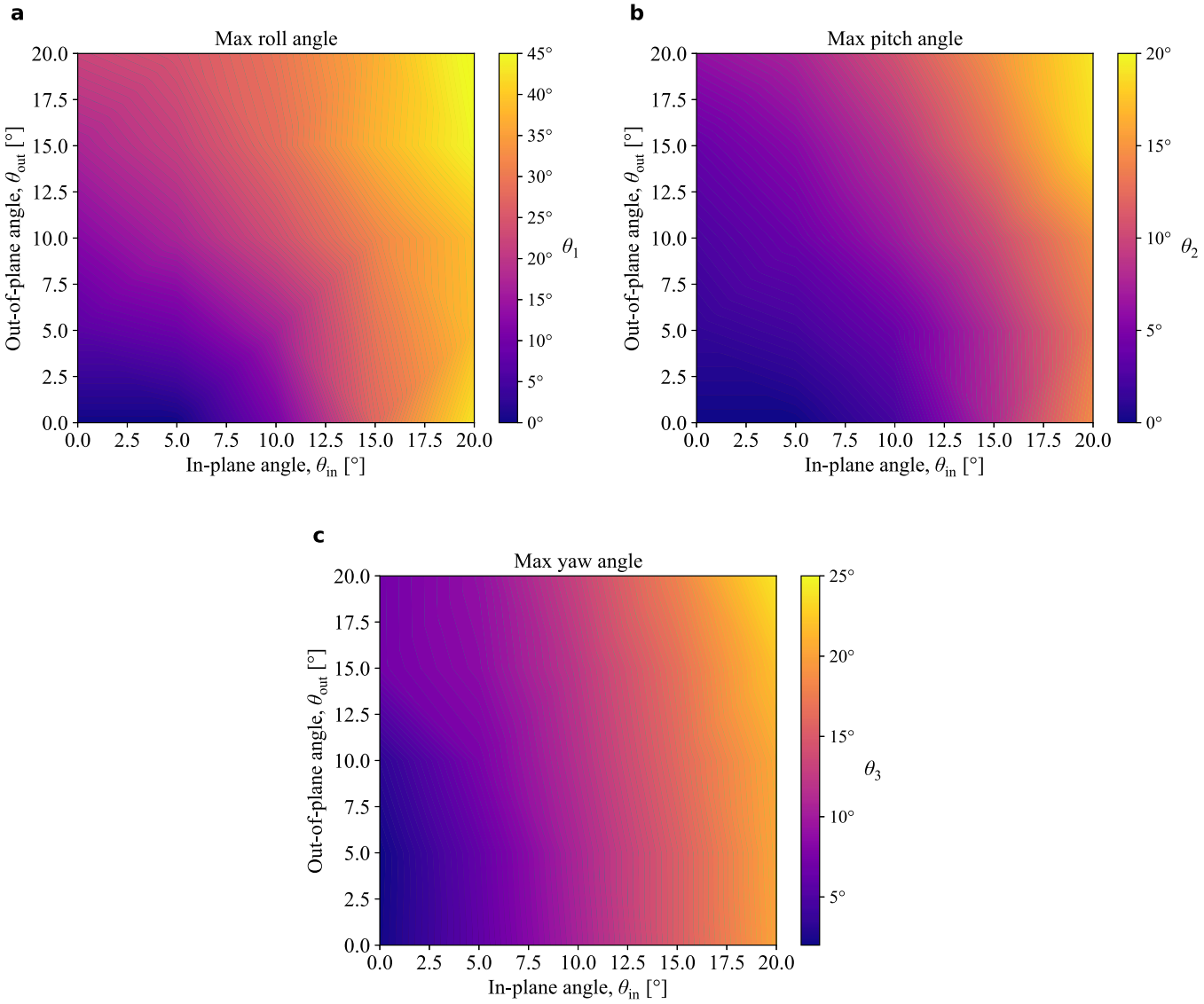

Figure 8. Maximum roll, pitch, and yaw amplitudes as a function of θ_{in} and θ_{out} for shapes with $a_s'/b_s' = 1.3$, $b_s'/c_s' = 1.2$, and $\Delta\bar{Y}' = 25$ m. Note the difference of the color bar scale.

uncertainty in the axis ratios, our estimate of ΔV_T from reshaping is, therefore, largely consistent with these recent reports, supporting the validity of our assumption. While the momentum enhancement factor β is also expected to be smaller than the initially reported value (i.e., $\beta = 3.61$ for the nominal system; Cheng et al. 2023), its uncertainty is primarily dominated by the current uncertainty in the mass of Dimorphos (Richardson et al. 2024). Consequently, Hera's measurements play a crucial role in refining β considering the reshaping effect. Importantly, we acknowledge the presence of factors other than reshaping, such as initial mass loss and subsequent accumulation of ejecta, which could also influence the orbit period of Dimorphos. However, compared to those effects, global-scale reshaping of Dimorphos is likely the dominant factor affecting the orbit period, second only to the momentum transfer itself.

Our investigation also highlights the significance of attitude perturbation induced by reshaping. Among the Euler angles describing Dimorphos's attitude state (roll, pitch, and yaw), the roll angle is prone to excitation under impact-induced reshaping. When reshaping was assumed to occur along the principal axes, most shapes remained attitude stable. The shapes with $b_s/c_s \sim 1.0$ led to an unstable roll, but pitch and yaw are relatively stable, known as the barrel instability (Ćuk et al. 2020). The shapes with $b_s/c_s < 1.0$ are always unstable in all three angles. Exactly at the estimated axis ratios, $a_s/b_s = 1.3$ and $b_s/c_s = 1.3$, reshaping-induced perturbation on attitude is likely negligible. However, even a slight change in the axis ratio within the current uncertainty could lead to an unstable attitude state, especially in the roll angle.

We also demonstrated that asymmetry resulting from off-principal-axis reshaping introduces further uncertainty in the attitude state. A stable shape under the axial reshaping can experience, for example, up to 50° in roll and about 25° in pitch and yaw angles under the presence of θ_{in} and θ_{out}. Because, in reality, the post-impact Dimorphos's shape likely has some degree of asymmetry, these results emphasize the practical difficulty in accurately predicting its attitude state. Furthermore, considering the additional impact-induced perturbations on Dimorphos's attitude, the likelihood of it entering a tumbling state (i.e., non-principal-axis rotation state) is increased. This has important implications for Hera, as its

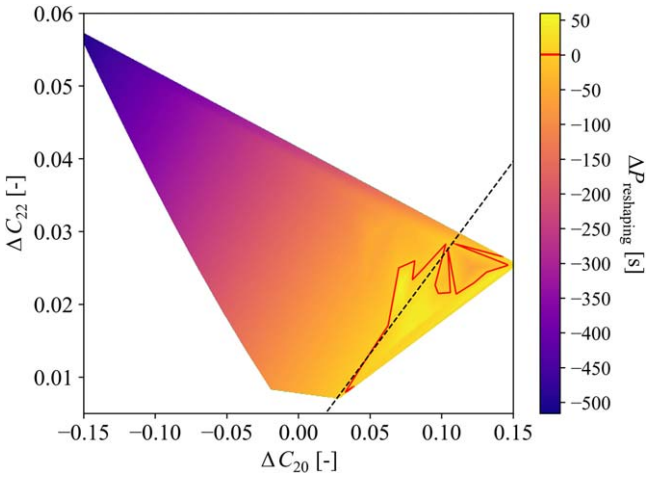

Figure 9. Reshaping-induced orbit period change, $\Delta P_{\mathrm{reshaping}}$, as a function of the changes in the zonal and tesseral terms of degree 2, ΔC_{20} and ΔC_{22}, respectively. Reshaping is assumed to occur along the principal axes, and the post-impact shape is symmetrical about the *Y*-axis, as shown in Figure 2. The red contour line indicates $\Delta P_{\mathrm{reshaping}} = 0$ s, while the dashed line denotes $\Delta C_{22} = 0.265\ \Delta C_{20}$, a theoretical boundary between positive and negative orbit period changes (Equation (B5)).

piggyback CubeSats, Juventas, and Milani, will orbit the Didymos system and land on the surfaces of the bodies (Michel et al. 2022). Detailed characterization of the system by Hera, Juventas, and Milani will provide further valuable insights into this complex binary system.

Acknowledgments

This work was supported in part by the DART mission, NASA contract 80MSFC20D0004 to JHU/APL. R.N. acknowledges support from NASA/FINESST (NNH20ZDA001N). S.D.R. and M.J. acknowledge support from the Swiss National Science Foundation (project number 200021_207359). P.M. acknowledges funding support from the French Space Agency CNES and The University of Tokyo. P.P. acknowledges support from the grant Agency of the Czech Republic, grant 23-04946S. S.R.S. acknowledges support from the DART Participating Scientist Program, grant No. 80NSSC22K0318. A.C.B. and P.Y.L. acknowledge funding by the NEO-MAPP project 717 GA 870377, EC H2020-SPACE-718 2018-2020/H2020-SPACE-2019, and by MICINN (Spain) PGC2021, PID2021-125883NB-C21. P.Y.L. acknowledges funding from the European Space Agency OSIP contract N.4000136043/21/NL/GLC/my. A portion of this work was carried out at the Jet Propulsion Laboratory, California Institute of Technology, under a contract with the National Aeronautics and Space Administration (No. 80NM0018D0004).

Appendix A
Simulation Setup

We perform the following four steps to prepare the system with reshaped Dimorphos that is initially dynamically equivalent to the nominal pre-impact system. These steps are also crucial to accurately describe the translational and attitude dynamics of the bodies within the simulation framework.

1. Generate a synthetic shape model of a reshaped Dimorphos.
2. Redefine (i.e., shift and rotate) the body-fixed frame such that it aligns with the principal moment of inertia axes.
3. Compute new initial angular velocity for Dimorphos.
4. Place the reshaped Dimorphos in the inertial frame such that its orientation with respect to Didymos is consistent with that of the pre-impact system.

In Step 1, we generate a synthetic shape model of the reshaped Dimorphos. As introduced in Section 2.2, reshaping of Dimorphos is characterized by modifying the axis lengths of a triaxial ellipsoid under the assumption that its volume remains constant. Note that the volume before reshaping V_{pre} is simply given by

$$V_{\mathrm{pre}} = \frac{4}{3}\,\pi\, a\, b\, c, \tag{A1}$$

where a, b, and c are the length of semiaxes. This equation, however, cannot be used to get the volume after reshaping V_{post} because positive and negative sides of the three axes are asymmetrically lengthened/shortened under the physically plausible impact-induced reshaping mode. Thus, we compute V_{post} by summing the volumes of tetrahedral FEM elements (e.g., Dobrovolskis 1996),

$$\begin{aligned} V_{\mathrm{post}} &= \sum_{i=1}^{N} v_i \\ &= \sum_{i=1}^{N} \frac{[\boldsymbol{n}_{i,2} - \boldsymbol{n}_{i,1}] \cdot ([\boldsymbol{n}_{i,3} - \boldsymbol{n}_{i,1}] \times [\boldsymbol{n}_{i,4} - \boldsymbol{n}_{i,1}])}{6}, \end{aligned} \tag{A2}$$

where v_i is the volume of element i, N is the total number of elements, and $\boldsymbol{n}_{i,1\ldots4}$ denotes the four nodes of element i.

After Step 1, the synthetic shape model is still described in the body-fixed frame of the pre-impact, unreshaped ellipsoid. In Step 2, we first shift the body-fixed frame's origin to the new center of mass location after reshaping. Subsequently, we rotate the frame to ensure that the moment of inertia tensor becomes diagonal in this new frame. Here, depending on the magnitude of reshaping, the intermediate and minor axes might be interchanged before and after reshaping.

Step 3 ensures the conservation of angular momentum. The initial angular velocity of Dimorphos after reshaping ω_{post} is straightforwardly determined by the equation

$$\omega_{\mathrm{post}} = I_{\mathrm{post}}^{-1}\, I_{\mathrm{pre}}\, \omega_{\mathrm{pre}}, \tag{A3}$$

where I is the moment of inertia tensor.

Finally, in Step 4, we place the reshaped Dimorphos in the inertial frame to match its orientation with the pre-impact state. As per the frame convention defined for the system (e.g., Richardson et al. 2024), the DART spacecraft approached along Dimorphos's intermediate axis from negative to positive direction as shown in Figure 2. It is crucial to ensure that, despite potential flips in the intermediate and minor axes after substantial reshaping, the original intermediate axis aligns with the impact vector and that the impact hemisphere faces Dimorphos's orbital direction, maintaining consistency with the head-on impact condition.

Appendix B
Changes in Degree 2 Zonal and Tesseral Terms of Dimorphos

The formulations and discussion here follow those presented in Nakano et al. (2022). The degree 2 spherical harmonics representation of the gravity potential of a spherical body is

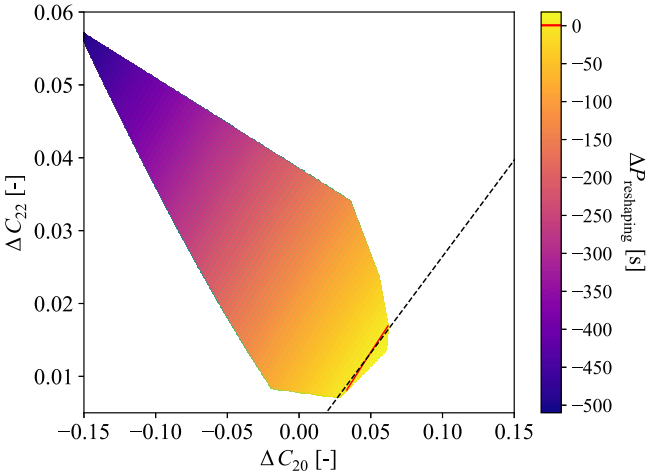

Figure 10. The same as Figure 9 but only for the shapes with $b_s/c_s > 1.0$.

given by

$$V_2 = -\frac{GM}{r}\left(\frac{a}{r}\right)^2 \sum_{m=0}^{2} P_{2m}\{C_{2m}\cos m\lambda + S_{2m}\sin m\lambda\}, \quad \text{(B1)}$$

where G is the gravitational constant, M is the mass of the body, a is the semimajor axis of a reference ellipsoid, r is the distance from coordinate origin to field point, λ is the longitude of field point, C_{2m} and S_{2m} are the spherical harmonics coefficients of degree 2 and order m, and P_{2m} are the associated Legendre functions of degree 2 and order m. In the frame aligned with the principal moments of inertia of the body, C_{21}, S_{21}, and S_{22} are identically zero, and thus, Equation (B1) can be simplified to

$$V_2 = -\frac{GM}{r}\left(\frac{a}{r}\right)^2 \left\{-\frac{1}{2}\,C_{20} + 3\,C_{22}\cos 2\lambda\right\}. \quad \text{(B2)}$$

The difference in Dimorphos's potential due to reshaping can be written as

$$\begin{aligned}\delta V_2 &= V_2^R - V_2^0 \\ &= -\frac{GM}{r}\left(\frac{a}{r}\right)^2 \left\{-\frac{1}{2}(C_{20}^R - C_{20}^0) + 3(C_{22}^R - C_{22}^0)\cos 2\lambda\right\} \\ &= -\frac{GM}{r}\left(\frac{a}{r}\right)^2 \left\{-\frac{1}{2}\,\Delta C_{20} + 3\,\Delta C_{22}\cos 2\lambda\right\},\end{aligned} \quad \text{(B3)}$$

where the superscripts 0 and R indicate the quantities for the nominal and reshaped cases, respectively. When there is no orbit period change, δV_2 is zero, and hence, the term inside the curly brackets in Equation (B3) must also be zero. Therefore, we have

$$\frac{\Delta C_{22}}{\Delta C_{20}} = \frac{1}{6\cos 2\lambda}. \quad \text{(B4)}$$

Given Dimorphos's reshaping mode considered in this work, ΔC_{22} is always positive. Thus, ΔC_{20} and $\cos 2\lambda$ should have the same sign when the equality in Equation (B4) holds. If we set $\cos 2\lambda$ to its mean value, we obtain

$$\Delta C_{22} = 0.265\,\Delta C_{20}, \quad \text{(B5)}$$

which represents the theoretical linear line for $\Delta P_{\rm reshaping} = 0$ s. Figure 10 presents $\Delta P_{\rm reshaping}$ only for the shapes with $b_s/c_s > 1.0$ (thus, there is no significant orbit period fluctuation owing to Dimorphos's attitude instability) as a function of ΔC_{20} and ΔC_{22}. In this case, the line given by Equation (B5) almost exactly aligns with the red contour line for $P_{\rm reshaping} = 0$ s.

ORCID iDs

Ryota Nakano https://orcid.org/0000-0002-9840-2416
Masatoshi Hirabayashi https://orcid.org/0000-0002-1821-5689
Sabina D. Raducan https://orcid.org/0000-0002-7478-0148
Petr Pravec https://orcid.org/0000-0001-8434-9776
Shantanu P. Naidu https://orcid.org/0000-0003-4439-7014
Harrison F. Agrusa https://orcid.org/0000-0002-3544-298X
Steven Chesley https://orcid.org/0000-0003-3240-6497
Fabio Ferrari https://orcid.org/0000-0001-7537-4996
Martin Jutzi https://orcid.org/0000-0002-1800-2974
Colby C. Merrill https://orcid.org/0000-0002-5566-0618
Alex J. Meyer https://orcid.org/0000-0001-8437-1076
Patrick Michel https://orcid.org/0000-0002-0884-1993
Derek C. Richardson https://orcid.org/0000-0002-0054-6850
Paul Sánchez https://orcid.org/0000-0003-3610-5480
Peter Scheirich https://orcid.org/0000-0001-8518-9532
Stephen R. Schwartz https://orcid.org/0000-0001-5475-9379
Yun Zhang https://orcid.org/0000-0003-4045-9046
Adriano Campo Bagatin https://orcid.org/0000-0001-9840-2216
Po-Yen Liu https://orcid.org/0000-0003-3929-0730
Andrew F. Cheng https://orcid.org/0000-0001-5375-4250

References

Agrusa, H. F., Gkolias, I., Tsiganis, K., et al. 2021, Icar, 370, 114624
Agrusa, H. F., Richardson, D. C., Davis, A. B., et al. 2020, Icar, 349, 113849
Barnouin, O., Ballouz, R.-L., Marchi, S., et al. 2023, NatCo, submitted
Chabot, N. L., Rivkin, A. S., Cheng, A. F., et al. 2024, PSJ, 5, 49
Cheng, A. F., Agrusa, H. F., Barbee, B. W., et al. 2023, Natur, 616, 457
Ćuk, M., Jacobson, S., & Walsh, K. 2020, EPSC Abstracts, 14, EPSC2020-983
Daly, R. T., Ernst, C. M., Barnouin, O. S., et al. 2023, Natur, 616, 443
Daly, R. T., Ernst, C. M., Barnouin, O. S., et al. 2024, PSJ, 5, 24
Davis, A. B., & Scheeres, D. J. 2021, GUBAS: General Use Binary Asteroid Simulator, Astrophysics Source Code Library, ascl:2107.013
Dobrovolskis, A. R. 1996, Icar, 124, 698
Ferrari, F., Panicucci, P., Merisio, G., et al. 2024, NatCo, submitted
Gao, Y., Yu, Y., Cheng, B., & Baoyin, H. 2021, AdSpR, 69, 2305
Hirabayashi, M., Davis, A. B., Fahnestock, E. G., et al. 2019, AdSpR, 63, 2515
Hirabayashi, M., Ferrari, F., Jutzi, M., et al. 2022, PSJ, 3, 140
Hirabayashi, M., Schwartz, S. R., Yu, Y., et al. 2017, MNRAS, 472, 1641
Hirabayashi, M., Raducan, S. D., Sunshine, J. M., et al. 2024, NatCo, submitted
Liu, P. Y., Campo-Bagatin, A., Benavidez, P. G., & Richardson, D. C. 2023, Icar, submitted
Maciejewski, A. J. 1995, CeMDA, 63, 1
Meyer, A. J., Agrusa, H. F., Richardson, D. C., et al. 2023b, PSJ, 4, 141
Meyer, A. J., Gkolias, I., Gaitanas, M., et al. 2021, PSJ, 2, 242
Meyer, A. J., Scheeres, D. J., Agrusa, H. F., et al. 2023a, Icar, 391, 115323
Michel, P., Küppers, M., Bagatin, A. C., et al. 2022, PSJ, 3, 160
Moreno, F., Bagatin, A. C., Tancredi, G., et al. 2023, PSJ, 4, 138
Naidu, S. P., Chesley, S. R., Moskovitz, N., et al. 2024, PSJ, 5, 74
Nakano, R., Hirabayashi, M., Agrusa, H. F., et al. 2022, PSJ, 3, 148
Pajola, M., Tusberti, F., Lucchetti, A., et al. 2024, NatCo, submitted
Pravec, P., Scheirich, P., Kušnirák, P., et al. 2006, Icar, 181, 63
Pravec, P., Scheirich, P., Kušnirák, P., et al. 2016, Icar, 267, 267
Raducan, S., Jutzi, M., Cheng, A., et al. 2024, NatAs, 8, 445
Raducan, S. D., & Jutzi, M. 2022, PSJ, 3, 128
Raducan, S.-D., Jutzi, M., Zhang, Y., Ormö, J., & Michel, P. 2022, A&A, 665, L10

Richardson, D. C., Agrusa, H. F., Barbee, B., et al. 2022, PSJ, 3, 157
Richardson, D. C., Agrusa, H. F., Barbee, B., et al. 2024, PSJ, submitted
Rivkin, A. S., Chabot, N. L., Stickle, A. M., et al. 2021, PSJ, 2, 173
Roth, N. X., Milam, S. N., Remijan, A. J., et al. 2023, PSJ, 4, 206
Scheeres, D. J. 2009, CeMDA, 104, 103
Thomas, C. A., Naidu, S. P., Scheirich, P., et al. 2023, Natur, 616, 448
Yu, Y., Cheng, B., Hayabayashi, M., Michel, P., & Baoyin, H. 2019, CeMDA, 131, 1
Zhang, Y., Michel, P., Richardson, D. C., et al. 2021, Icar, 362, 114433
Zhang, Y., Richardson, D. C., Barnouin, O. S., et al. 2017, Icar, 294, 98